Characterization of Inertial Sensor Measurements for Navigation Performance Analysis

John H. Wall and David M. Bevly
GPS and Vehicle Dynamics Lab, Department of Mechanical Engineering, Auburn University

BIOGRAPHY

John H. Wall received his B.S. in Mechanical Engineering from Christian Brothers University, and is currently an M.S. candidate in the department of Mechanical Engineering at Auburn University. His focus as a research assistant with the GPS and Vehicle Dynamics Laboratory at Auburn involves the characterization of inertial sensors for the purpose of studying the effects of errors in the computation of navigation solutions.

David Bevly received his B.S. from Texas AM University in 1995, M.S from Massachusetts Institute of Technology in 1997, and Ph.D. from Stanford University in 2001 in Mechanical Engineering. He joined the faculty of the Department of Mechanical Engineering at Auburn University in 2001 as an assistant professor. Dr. Bevly is the director of Auburn University's GPS and Vehicle Dynamics Laboratory which focuses on the control and navigation of vehicles using GPS in conjunction with other sensors, such as Inertial Navigation System (INS) sensors.

ABSTRACT

This paper develops analytical and empirical bounds on the inertial sensor error growth due to the numerical integration of rotation rate and acceleration outputs of various grade inertial measurement units (IMU). The developed error bounds provide an explicit measure of the performance of the IMU when it is the sole means of navigation. Accurate analysis of inertial sensor error growth is essential to ensuring the effectiveness of the optimal synergy of GPS and inertial measurements, as success is often limited by the availability of GPS signals in harsh environments. Studies of inertial sensors and their associated error modes have been developed resulting in the wide use of these models for use in GPS/INS algorithms. This paper presents an analysis of the IMU models to investigate the behaviors of inertial navigation error growth due to the subsequent integrations of the raw measurements in dead reckoning. The main purpose of this study is to provide quantitative specification on the degradation of navigation solutions when dead reckoning with IMUs. The parameters characterizing the sensor models for which the error analysis is performed are identified using autocorrelation and Allan variance techniques and the resulting analytical based formulations are validated using Monte Carlo simulation methods.

INTRODUCTION

The stochastic errors present on inertial sensors cause the subsequent numerical integrations of the measurements to exhibit an ever increasing variance. That is, when a gyro or accelerometer output is numerically integrated in a dead-reckoning navigator, the variance in the resulting position and velocity outputs grow unbounded in time. This degradation of measurement accuracy propagates into the navigation solution (ie. position and velocity in the earth frame) at rates dependent on the integrity of the component sensors, the algorithms employed, and the duration of the un-aided navigation.

Inertial navigation uncertainty during dead reckoning through GPS outages has been a pertinent topic in the realm of GPS/INS fusion as many such integration systems use an IMU as the sole means of estimation during GPS failure. Accurate bounds or expectation of the uncertainty of the inertial-derived position, velocity, are needed to best characterize inertial systems as it is these integral values which are of interest in navigation. The standard specifications given for an inertial system are those pertaining to the raw accelerations and rotation rates, not the navigation-pertinent integral values. The specifications of the raw inertial measurement stochastic errors do not fully depict its performance in its wide-use as a means to navigate. The expected accuracy of a dead reckoning system depends on the quality of the particular

IMU used, the varieties of which have error characteristics specific to the make and model. To accurately compare and distinguish the performance of varieties of IMUs in dead-reckoning, an analysis of the integrated inertial measurements is imperative.

The main goal of this work is to provide explicit, closed-form expressions which characterize the behaviors of the dead reckoning error growth in time as a function of identifiable error parameters. The closed-formed expressions presented in this work provide a standard deviation, or expected uncertainty due to the numerical integration of two major inertial error sources: wide-band noise and bias drift.

SIMPLE SENSOR MODELS

The measurement model for an accelerometer is given as:

$$a = \ddot{x} + \omega_a + b_a \tag{1}$$

$\ddot{x}$ is the true acceleration
ω_a is zero mean wide-band noise with variance σ_a^2
b_a is the bias drift

Similarly, the measurement model for a rate gyro is given as:

$$g = \dot{\psi} + \omega_g + b_g \tag{2}$$

$\dot{\psi}$ is the true angular velocity
ω_g is zero mean wide-band noise with variance σ_a^2
b_g is the bias drift

The bias drift in each of the above equations is commonly modeled as a 1st order Gauss-Markov process:

$$\dot{b} = \frac{-b}{\tau} + \omega_b \tag{3}$$

τ is the time constant or correlation time
ω_b is zero mean wide-band noise with variance $\sigma_{b_a}^2$

The preceding sensor models have been widely used in the navigation community as sufficient models of the static stochastic errors of accelerometers and gyroscopes. The following models do not include terms associated with environmental effects (temperature) or dynamic motion (scale factor) as these errors are assumed to be deterministic or able to be removed by preliminary calibration methods. Additionally, the constant turn-on bias is neglected in this study as it is readily identified and removed during calibration. The statistical parameters describing the stochastic errors present in these models are assumed to be constant; the statistic processes are assumed to be stationary. The effects of temperature, dynamic motion, and sensor installation are assumed to be well known and compensated using deterministic calibration procedures.

IDENTIFICATION OF MODEL PARAMETERS

The statistical parameters in the preceding sensor models can be estimated using various identification techniques. Such techniques include Allan variance charts, autocorrelation functions, and Monte Carlo simulations.

The wide band noise is commonly characterized by the random walk parameter, a standard deviation normalized to sampling frequency. The value of random walk parameter is easily determined from the standard deviation of a sufficiently long static data set. The Allan variance technique also yields the specification for angular or velocity random walk; it is the value of the Allan variance corresponding to a 1 second averaging time.

The 1st order markov process has a known autocorrelation form and is given below:

$$R_{xx}(T) = {\sigma_b}^2 e^{-T/\tau} \tag{4}$$

τ is the time constant or correlation time
σ_b is the variance of the markov process, b

Assuming the bias drift exhibits the Gauss-Markov model form, the time constant and variance can be recovered from experimental autocorrelation data. [3] and [2] have used knowledge of this form and numerical autocorrelation data from detrended sensor outputs to identify the time constant and variance of the bias drift component. The raw sensor measurement, corrupted by both noise and drift, must first be filtered to remove the higher frequency noise, thus isolating the drifting bias component. Reasonable accuracy of the autocorrelation technique necessitates having a data set many times longer than the time constant of the process; the accuracy of an autocorrelation 'match' is directly related to the amount of data being processed and the inherent parameters attempting to be identified.[4] Figure 1 illustrates a comparison of a numerical autocorrelation of simulated markov process data and its analytical curve as described by equation (4). The plot shows that the autocorrelation of simulated Markov data match the analytical expression with the known markov parameters.

The Allan variance, first introduced in [5] as a means to quantify the precision of atomic oscillators, can be used to identify all parameters necessary to fully model and emulate a sensor exhibiting the certain model forms described by equations (1-3). The Allan variance quantifies the various stochastically-driven error sources present on an inertial sensor output and is best represented on a log-log plot. Figure 2 is an Allan variance plot of simulated sensor data using the simple model form in (2) with specs similar to that of a low grade rate gyro. The different slopes seen

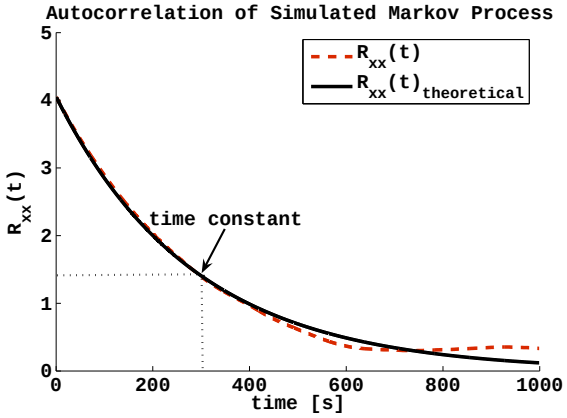

Fig. 1 Autocorrelation of Markov data simulated with $\sigma^2 = 4, \tau = 300$

on the plot indicate the unique regions dominated by the sensor's consituent sources. The analytical line is the expected curve based on the same sensor specifications used to simulate the data. The initial downward slope indicates the sensor's primary error source is angular random walk, or white noise, where for higher averaging times, the variance increases with a convex down shape, indicating the dominant error source is exponentially correlated noise, otherwise known as a Gauss-Markov process.

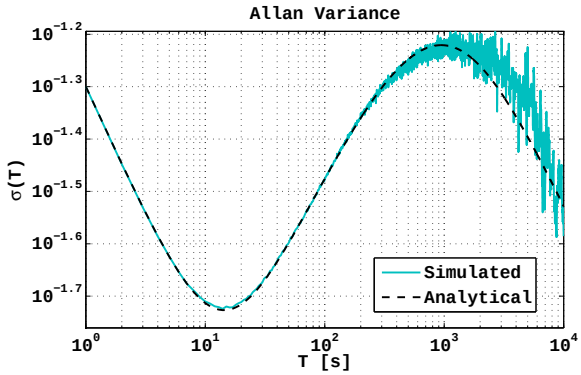

Fig. 2 Allan Variance: Sample Gyro

Analytical expressions of the Allan variance for common noise sources have been derived from each source's relationship to the power spectral density in [6]. Curve-fitting techniques have utilized the analytical expressibility of the Allan variance for the extraction of the statistical parameters associated with inertial sensor error sources. Such techniques have been employed to ascertain the various inertial sensor specifications describing the noises present.[7] The extracted parameters from the Allan variance curve-fits can be used for the accurate analysis of inertial sensor behavior as implemented in navigation.

The Allan variance plot in figure 3 shows both a simulated low grade and a high grade gyro each generated with the simple model and specifications as listed in common sensor spec sheets. As can be seen on the loglog graph, the high grade sensor has an overall lower variance magnitude than the low grade sensor and its constant downward slope indicates that the bias drift is less present than with the cheaper sensor. The stability of such a high grade gyro results in a straight line allan variance, where as a lower grade sensor typically shows an eventual positive slope indicative of its prevalent bias drift characteristic.

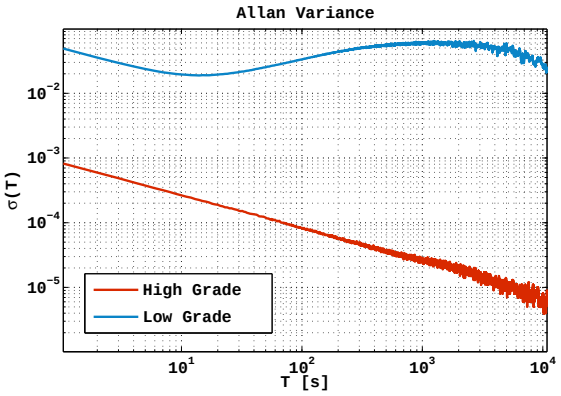

Fig. 3 Allan Variance: Gyro Grade Comparison

VALIDATION OF MODELS

The statistical parameters ascertained with the preceding techniques are used to simulate sensor data for comparison to the experimental data from the actual sensors. The Allan variance plot of simulated and experimental data is expected to show minimal discrepancy if the simulated model has captured the characteristics exhibited in the actual model. The following analysis assumes the preceding sensors models are valid and the specifications describing the model terms can be found using such techniques.

ERROR GROWTH ANALYSIS

The integration of the bias drift and wide-band noise error sources can each be quantified as a having characteristic variance growth in time. Since the two sources under investigation are completely uncorrelated, the variance of each integrated error source can be analyzed independently and summed to yield a final integrated sensor variance. Following each derivation is a plot of both the analytical expression and the Monte Carlo simulation serving to depict the behavior of the integrated error sources and validate the analysis.

Variance of single-integrated wide-band noise

The variance of single-integrated wide-band noise has been shown in [9] to have a variance with the characteristic growth as a function of the variance of the wide-band noise and sample rate:

$$\sigma_{\dot{y}}^2 = \sigma_{\omega}^2 \Delta t^2 k \tag{5}$$

Figure 4 shows the behavior of the square root of derived equation (5), the standard deviation of integrated wide-band noise.

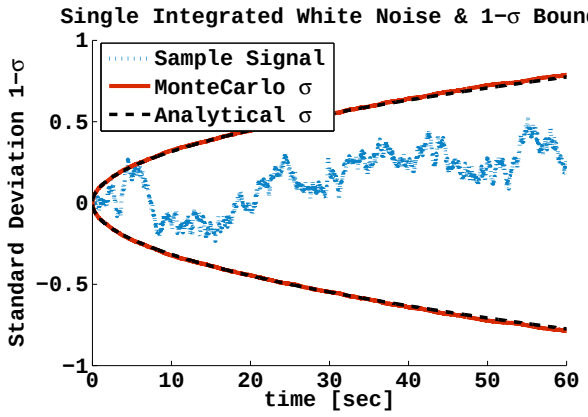

Fig. 4 Single Integrated Wide-Band Noise

Variance of double-integrated wide-band noise

Using a similar approach to the author of expression (5), the variance of a second integration of wide-band noise is derived as follows. This variance represents the body-frame position error contribution of wide-band noise on an accelerometer measurement.

Let $\ddot{y}$ represent the generic measurement corrupted only with wide-band noise, ω

$$\ddot{y} = \omega \tag{6}$$

Double integrating the $\ddot{y}$ measurement results in the position.

$$y = \int \dot{y}\, dt = \int \int \omega\, dt\, dt \tag{7}$$

Approximate the integration by employing Euler's method and substitute the summation for single integrated white noise.

$$\begin{aligned} y_k &= y_{k-1} + \Delta t \dot{y}_{k-1} \\ y_k &= y_0 + \Delta t^2 \sum_{j=0}^{k-1} \left(\sum_{i=0}^{j-1} \omega_i \right) \end{aligned} \tag{8}$$

Express the nested summations as a single summation with a coefficient

$$y_k = \Delta t^2 \sum_{i=0}^{k-1} (k - j - 1)\, \omega_i \tag{9}$$

Square and take the expected value of both sides with knowledge that successive ω values in time are completely uncorrelated

$$\mathrm{E}\left[y_k y_k\right] = \Delta t^4 \sum_{j=0}^{k-1} (k - j - 1)^2 \mathrm{E}\left[\omega_i \omega_i\right] \tag{10}$$

Expansion and simplification yields an expression for the variance of double integrated wide-band noise as a function of the noise variance, time, and sampling interval.

$$\sigma_y{}^2 = \Delta t^4 \sigma_\omega{}^2 \left(\frac{1}{6} k(k+1)(2k+1) \right) \tag{11}$$

Figure 5 depicts the behavior of equation (11) and shows that the analytical expression matches the Monte Carlo computation with simulated data. The simulated data was generated with 2000 Monte Carlo iterations.

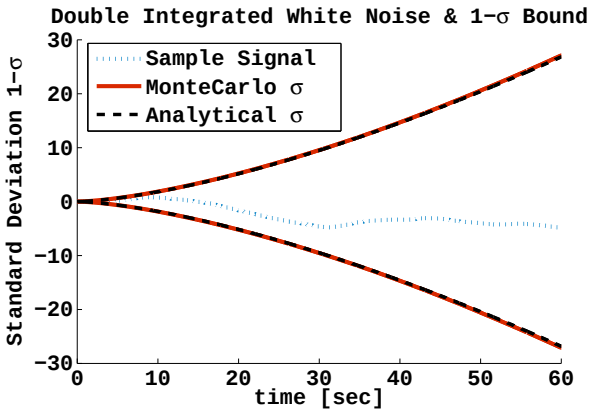

Fig. 5 Double Integrated White Noise

Variance of 1st order Gauss-Markov process

As an instructive measure for subsequent derivations, the authors show the variance of the un-integrated Markov process, or sensor drift, as it is present on raw inertial measurements.

The differential equation for the 1st order Gauss-Markov process as given in equation (3) can be solved using the following Euler integration scheme:

$$\begin{aligned} b_k &= b_{k-1} + \Delta t \dot{b}_{k-1} \\ b_k &= \left(1 - \frac{\Delta t}{\tau}\right) b_{k-1} + \Delta t \omega_{k-1} \end{aligned}$$

For clarity in derivation let $A = \left(1 - \frac{\Delta t}{\tau}\right)$,

$$b_k = Ab_{k-1} + \Delta t \omega_{k-1} \tag{12}$$

The expression above is written as the following summation with initial condition $b_0 = 0$

$$b_k = \Delta t \sum_{i=0}^{k-1} A^{k-i-1} \omega_i \tag{13}$$

Square both sides and take the expected value of both sides with knowledge that successive ω values in time are completely uncorrelated

$$\mathrm{E}\left[b_k b_k\right] = \Delta t^2 A^{2k-2} \sum_{i=0}^{k-1} A^{-2i} {\sigma_\omega}^2 \tag{14}$$

Use the solution to the geometric series to yield the following analytical expression

$$\mathrm{E}\left[b_k b_k\right] = \Delta t^2 A^{2k-2} \left(\frac{1 - A^{-2k}}{1 - A^{-2}}\right) {\sigma_\omega}^2 \tag{15}$$

The resulting expression is the variance of a 1st order Gauss-Markov process as a function of the variance of the driving noise, time, and sampling interval.

$${\sigma_b}^2 = \Delta t^2 {\sigma_\omega}^2 \left(\frac{A^{2k} - 1}{A^2 - 1}\right) \tag{16}$$

Variance of single-integrated 1st order Gauss-Markov process

The following derivation will provide the variance due to the single integration of a Gauss Markov process. This result will be the contribution to the error uncertainty in body frame velocity/attitude-angle derived from an accelerometer/gyro measurement due to the bias drift error source.

Let $\ddot{x}$ represent the bias drift as the solution of equation (3)

$$\ddot{x}_k = b_k = Ab_{k-1} + \Delta t \omega_{k-1} \tag{17}$$

Approximate the integral using Euler's method using initial condition $\dot{x}_0 = 0$

$$\begin{aligned} \dot{x} &= \int \ddot{x}\, dt = \int b\, dt \\ \dot{x}_k &= \dot{x}_{k-1} + \Delta t \ddot{x}_{k-1} \\ \dot{x}_k &= \Delta t^2 \sum_{j=0}^{k-2} \left(\sum_{i=0}^{j} A^j A^{-i} \omega_i \right) \end{aligned} \tag{18}$$

The above summation can be more conveniently expressed as

$$\dot{x}_k = \Delta t^2 \sum_{i=0}^{k-2} \omega_i \left(\sum_{j=0}^{k-1-i} A^j \right) \tag{19}$$

This form can then be reduced to a single summation through knowledge of the solution to the geometric series

$$\dot{x}_k = \frac{\Delta t^2}{1 - A} \sum_{i=0}^{k-2} \left(1 - A^{k-1-i}\right) \omega_i \tag{20}$$

Square and take the expected value of both sides with knowledge that successive ω values in time are completely uncorrelated

$$\mathrm{E}\left[\dot{x}_k \dot{x}_k\right] = \frac{\Delta t^4}{(1 - A)^2} \sum_{i=0}^{k-2} \left(1 - A^{k-1-i}\right)^2 \mathrm{E}\left[\omega_i \omega_i\right] \tag{21}$$

Expansion and simplification of the above expression yields the expression for the variance of once integrated 1st order Gauss-Markov process

$${\sigma_{\dot{x}}}^2 = \Delta t^4 {\sigma_\omega}^2 \left(\frac{1 + 2A - 2A^k - 2A^{1+k} + A^{2k} - k + kA^2}{-1 + 2A - 2A^3 + A^4}\right) \tag{22}$$

Which reduces to a simple form:

$${\sigma_{\dot{x}}}^2 = \Delta t^4 {\sigma_\omega}^2 \left(-c_1 + c_2 A^k - c_3 A^{2k} + c_4 k\right)$$

where $c_1, c_2, c_3,$ andc_4 are positive constants

Figure 6 below shows that the variance from the derived expression (22) match a Monte Carlo simulation with 2000 iterations. This Markov data is simulated using arbitrary specifications.

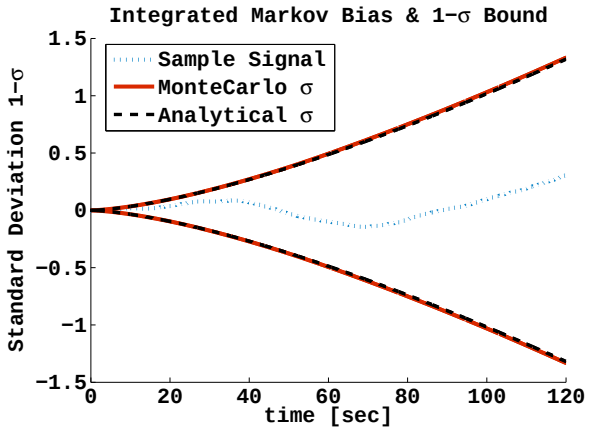

Fig. 6 Integrated Markov Process

The standard deviation of an integrated inertial sensor as modeled by equation (1) or (2) is simply the square root of the sum of the variances of each of the integrated error sources as in (5) and (22) . This is shown in equation form as:

$$\sigma_{\int Sensor} = \sqrt{{\sigma_{\dot{x}}}^2 + {\sigma_{\dot{y}}}^2} \tag{23}$$

Figure 7 shows the behavior of equation (23) validated with its match to the Monte Carlo simulation.

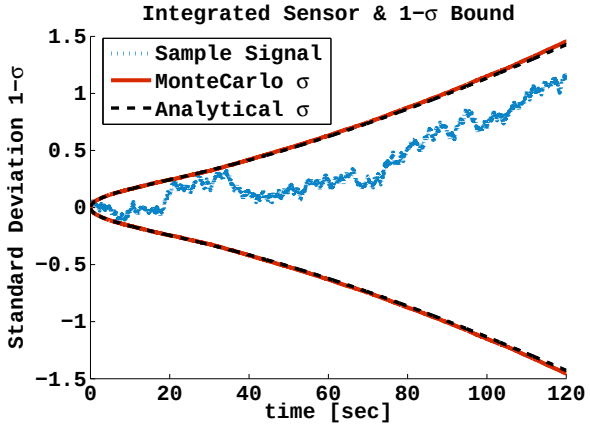

Fig. 7 Integrated Sensor Measurement

Figure 8 shows the 1-σ curves of each of the different error sources and the resulting combination of both errors. This particular plot shows the relative and total effect of the bias drift and white noise components on the estimated angle or velocity. After some time, the integrated bias drift begins to dominate as the larger source of error. Due to the integrated Markov's fast growing variance even a relatively small bias drift can have large effects on the integrated accuracy especially for long times.

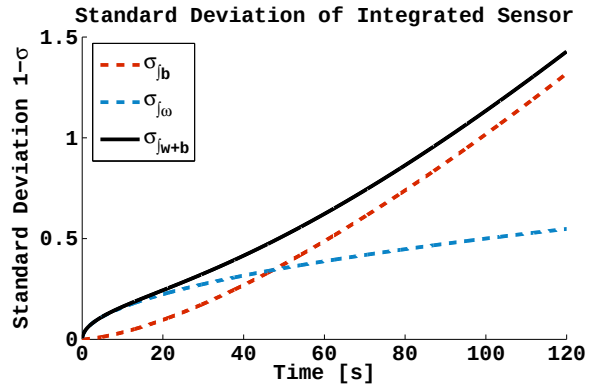

Fig. 8 Error Source Contribution

Variance of double-integrated 1st order Gauss-Markov process

The following derivation will provide the variance due to the double integration of a Gauss Markov process. This result will be the contribution to the error uncertainty in body frame position derived from an accelerometer measurement due to the bias drift error source.

Let x represent the double integrated sensor drift model

$$x = \int \dot{x}\, dt = \int \left(\int b\, dt \right) dt$$

The double Euler integration of the bias drift, $\dot{x}$, is represented below as a series of nested summations using the initial condition $x_0 = 0$

$$x_k = \Delta t^3 \sum_{m=0}^{k-1} \sum_{j=0}^{m-1} \sum_{i=0}^{j-1} A^{j-i-1} \omega_i \tag{24}$$

Simplify the triple summation expression into two nested summations in which ω_i is removed from the innermost summation.

$$x_k = \Delta t^3 \sum_{i=0}^{k-3} \omega_i A^{k-3-i} \sum_{j=0}^{k-3-i} \left(jA^{-j} + A^{-j} \right) \tag{25}$$

Substitute to decouple the iA^{-i} term.

$$x_k = \Delta t^3 \sum_{i=0}^{k-3} \omega_i A^{k-3-i} \left(\sum_{j=0}^{k-3-i} A^{-j} - A \frac{d}{dA} \sum_{j=0}^{k-3-i} A^{-j} \right) \tag{26}$$

Simplify and take the derivative. The form reduces to

$$x_k = \Delta t^3 \sum_{i=0}^{k-3} \omega_i \frac{(A^{k-1-i} + A - 2 - kA + k + iA - i)}{(A-1)^2} \tag{27}$$

Square and take the expected value of both sides with knowledge that successive ω values in time are completely uncorrelated

$$\mathrm{E}[x_k x_k] = \Delta t^3 \sum_{i=0}^{k-3} \mathrm{E}[\omega_i \omega_i] \frac{(A^{k-1-i} + A - 2 - kA + k + iA - i)^2}{(A-1)^4} \tag{28}$$

The final result is an expression for the variance of a double integrated Markov process in terms of the sampling interval, time constant, variance of the Markov driving noise, and time

$$\begin{aligned} {\sigma_x}^2 \;=\; & \Delta t^3 {\sigma_\omega}^2 \Big(c_1 k^3 + \\ & c_2 k^2 + \\ & (c_3 + 12A^k - 12A^{2+k}) k + \\ & (c_4 - 12A^k + 12A^{2+k} + 6A^{2k}) \Big) \end{aligned} \tag{29}$$

where,

$$\begin{aligned} c_1 &= -2 - 4A + 2A^4 + 4A^3 + 2 \\ c_2 &= 9 - 12A - 6A^2 + 12A^3 - 3A^4 \\ c_3 &= -13 + 8A - 8A^3 + A^4 \\ c_4 &= 6 - 12A^2 \end{aligned}$$

Figure 9 below shows that the variance from the derived expression (30) match a Monte Carlo simulation with 2000 iterations. This Markov data is simulated using arbitrary specifications.

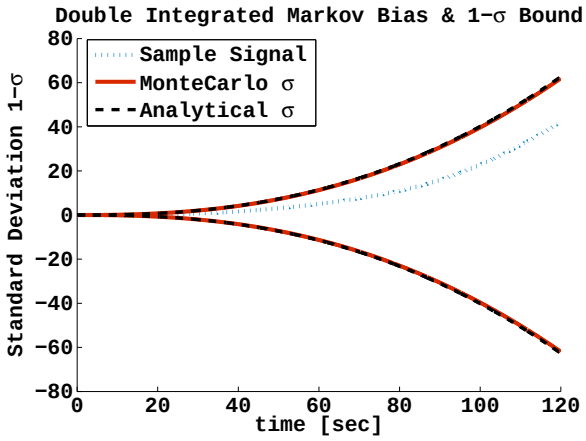

Fig. 9 Double Integrated Markov Process

The standard deviation of an double integrated accelerometer as modeled by equation (1) is simply the square root of the sum of the variances of each of the integrated error sources as in (11) and (30). This is shown in equation form as:

$$\sigma_{\int\int Sensor} = \sqrt{{\sigma_x}^2 + {\sigma_y}^2} \tag{30}$$

Figure 10 shows the behavior of equation (30) validated with its match to the Monte Carlo simulation.

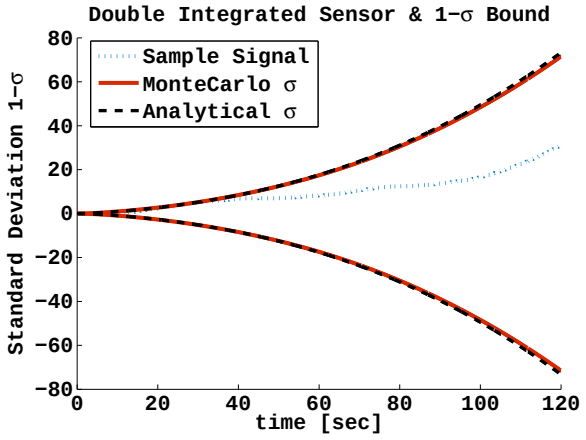

Fig. 10 Double Integrated Sensor Measurement

Figure 11 shows the different 1-σ curves of the different error sources and the resulting combination of both errors. This particular plot shows the relative and total effect of the bias drift and white noise components on the position from an double integrated accelerometer. As with the single integrated sensor, the double integrated sensor's bias drift begins to dominate as the larger source of error for longer integration times. It is evident that the accuracy of an inertially-derived position is highly sensitive to even small amounts of bias drift.

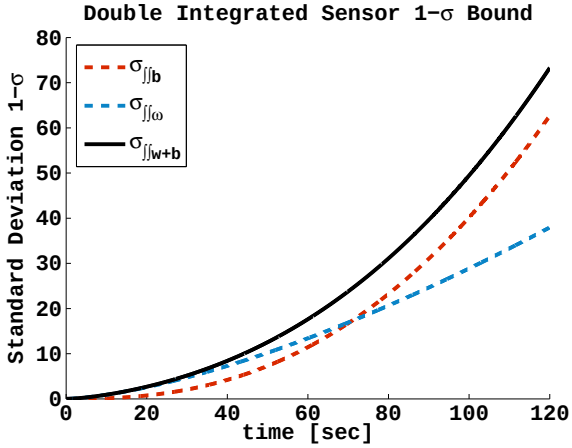

Fig. 11 Error Source Contribution

CONCLUSIONS

The derivations presented in this work quantify the inertial navigation accuracy due to the integration of white noise and exponentially correlated noise on rotation rate and accelerometer measurements. The variances expressions describe, in terms of known sensor specifications, the expected uncertainty of inertial-derived body-frame velocity, position, and attitudes over a certain integration time interval. This information may prove useful for direct and dynamic comparison of the performance of multiple inertial systems and their respective dead-reckoning accuracy. In GPS/INS based navigators these analytical results provide quick and valid predictions of the robustness of the systems when GPS is unavailable for specified lengths of time. This quantification proves especially useful when choosing components of such a navigation system or designing accurate fault-detection modes for such inertial-aided devices.

As the production of valid error growth curves for a given set of inertial sensors depends highly on accurate identification of sensor parameters and as full identification is not always possible, these curves may be constructed with conservative parameter estimates to provide a safe expected bound. In cases where other error sources due to temperature and dynamics are not fully known, these curves may provide a rough estimate or best-case scenario quantification of sensor performance.

Although this paper has provided specific expectations on accuracy based on specific inertial error sources, additional

work is recommended to include investigation into the effects of other stochastic error sources, such as bias instability and scale factor drift, on the variance of the resulting signal. Variance derivations with other sensors such as map-systems, vision, and odometry can prove usefule for the comparison of many such systems in use. It is recommended that further analysis be performed to yield the analytical propagation of errors from the combination of multi-sensor systems into the navigation or global reference frame.

A comparative study of alternative bias drift models or further validation of the Markov model as well as additional dead-reckoning experiments with multiple grade sensors is a must in proving the utility of the variance information. As static identification procedures can not always accurately characterize the sensor errors, useful future studies should include a sensitivity analysis to determine the effect of individual error source parameters on the variance growth. In addition [10] has shown that the stochastic errors on inertial sensors change considerably over the operating range of the device. It is recommended that the preceding analysis be expanded to study the effects of such trends and uncertainties associated with dynamic motion and temperature to improve the validity of the analysis presented in this work.

REFERENCES

[1] Gelb A., Applied Optimal Estimation. The MIT Press, Cambridge, Massachusetts, 1974.

[2] Gebre-Egziabher D., "Design and Performance Analysis of a Low-Cost Aided Dead Reckoning Navigator." A Dissertation submitted to the Department of Aeronautics and Astronautics and the Committee on Graduate Studies of Stanford University, Stanford University 2003.

[3] Flenniken W.S. IV., "Modeling Inertial Measurement Units and Analyzing the Effect of Their Errors in Navigation Applications." A Thesis submitted to the Department of Mechanical Engineering and the Committee on Graduate Studies of Auburn University, Auburn University 2005.

[4] Brown R.G., Hwang P. Introduction to Random Signals and Applied Kalman Filtering. Wiley, New York, 1997.

[5] Allan D.W., "Statistics of Atomic Frequency Standards." Proceedings of the IEEE, 54(2): 221, February 1966.

[6] Tehrani, M.M. "Ring Laser Gyro Data Analysis With Cluster Sampling Technique." Proceedings of SPIE - The International Society for Optical Engineering, v412: 207-220, 1983.

[7] Grantham B. E.,Bailey M. A., "A Least-Squares Normalized Error Regression Algorithm with Application to the Allan Variance Noise Analysis Method." Proceedings of The Institute of Navigation's Position and Location Symposium, San Diego, CA, April 2006.

[8] Gebre-Egziabher D., Powell J. D., "A DME Based Navigator for General Aviation Applications During the Transition to a Sole-Means GPS National Aerospace System." Proceedings of the Institute of Navigation's National Technical Meeting, Anaheim, CA, January, 2000.

[9] Flenniken W. S. IV., "Characterization of Various IMU Error Sources and the Effect on Navigation Performance." Proceedings of The Institute of Navigation's GNSS Meeting, Long Beach, CA, September 2005.

[10] Pethel, S. J., "Test and Evaluation of High Performance Micro Electro-Mechanical System Based Inertial Measurement Units." Proceedings of The Institute of Navigation's Position and Location Symposium, San Diego, CA, April 2006.